JOURNAL OF Materials CHEMISTRY

# Modulated charge ordering process in $Sm_{0.5}Ca_{0.5}Mn_{1-x}Cr_xO_3$ manganites

**A. Barnabé, M. Hervieu, C. Martin, A. Maignan and B. Raveau**

*Laboratoire CRISMAT, ISMRA—UMR 6508, Université de Caen, 6 Boulevard du Maréchal Juin, 14050 Caen Cedex, France*

The oxides $Sm_{0.5}Ca_{0.5}Mn_{1-x}Cr_xO_3$, with $0 \leqslant x \leqslant 0.07$, have been studied by electron diffraction and electron microscopy *versus* temperature from 90 K to 300 K, in connection with their magnetic and transport properties. An incommensurate charge ordering appears at $T_{CO} = 275$ K for the undoped compound, then a progressive transition from an incommensurate to a commensurate modulated structure is observed as $T$ decreases from 275 K to 170 K. But the most important point is that chromium doping enhances the incommensurability of the structure: the $q$ vector of the low temperature form decreases and $T_{CO}$ decreases abruptly as the chromium content $x$ increases, so that the charge ordering process is weakened and finally disappears for $x = 0.05$. The structure of the low temperature form of these manganites is characterized by a double supercell, $2a_p\sqrt{2} \times 2a_p \times a_p\sqrt{2}$, similar to that observed for other $Ln_{0.5}Ca_{0.5}MnO_3$ manganites with Ln = La, Pr, Nd, Tb. However, in these series, one observes similar space groups (*P2mm* or *Pmmm*) for Ln = Nd, Sm, different from those observed for Ln = La, Tb.

## Introduction

In the large series of manganites $Ln_{1-x}A_xMnO_3$ with A = Ca, Sr, Ba, Pb which exhibit colossal magnetoresistance (CMR) properties, those with $x = 0.5$ have been the subject of numerous studies in recent years, owing to their great complexity. The compounds $Ln_{0.5}A_{0.5}MnO_3$ display a great variety of magnetic structures, and charge ordering phenomena (ordering of $Mn^{3+}$ and $Mn^{4+}$ species over the lattice) have been shown to influence their magnetotransport properties.[1–4] The average size of the interpolated cation and the mismatch between the A-site cations were found to be the factors which govern the magnetotransport properties.[3,5–9] For the $x = 0.5$ oxides, a doubling of the $a$ parameter is observed at low temperature.[1,10–14] However, the ordering process is complex, *i.e.* it was shown that the antiferromagnetic (AFM) to ferromagnetic (FM) transition in $La_{0.5}Ca_{0.5}MnO_3$ is accompanied by a commensurate to incommensurate charge-ordering transition.[10,11]

Among these manganites, the phases with small A-site cations, such as $Sm_{0.5}Ca_{0.5}MnO_3$, are of great interest although they are semiconductors and do not exhibit any CMR effect in applied magnetic fields of up to 7 T.[15,16] Indeed, the doping of these manganites by chromium, cobalt or nickel allows CMR properties to be induced.[16–18] At this point of the studies, it is of major importance to try to understand the relationship between the magnetotransport properties of these materials and the charge ordering phenomena that appear *versus* temperature.

In the present paper, we show for the first time that chromium doping increases the incommensurability of the structure and decreases $T_{CO}$, charge ordering disappearing abruptly for very low chromium content ($x \approx 0.05$). Moreover, we demonstrate that $Sm_{0.5}Ca_{0.5}MnO_3$ exhibits a low temperature structure different from other $Ln_{0.5}Ca_{0.5}MnO_3$ manganites with Ln = La, Tb, characterized by the absence of a $2_1$ axis.

## Experimental procedure

Polycrystalline samples were synthesised from stoichiometric mixtures of $Sm_2O_3$, CaO, $Cr_2O_3$ and $Mn_2O_3$, according to the title composition $Sm_{0.5}Ca_{0.5}Mn_{1-x}Cr_xO_3$. For the present study, the chromium content, $x$, was varied from 0 to 0.07 in steps of 0.01. The mixtures were first heated to achieve decarbonation, sintered at 1500 °C for 12 hours and slowly cooled to room temperature.

The electron diffraction (ED) study at room temperature was performed with a JEOL 200CX electron microscope fitted with a tilting-rotating sample holder (tilt $\pm 60°$ and rotation $\pm 180°$). The ED study *versus* temperature and the bright/dark field imaging were carried out with a JEOL 2010 electron microscope fitted with a double tilt cooling sample holder ($\pm 40°$ and with $92\ K < T < 300\ K$). The ED patterns were recorded *versus* $T$ keeping a constant electron current density. The high resolution electron microscopy study was made with a TOPCON 002B electron microscope operating at 200 kV ($C_s = 0.4$ mm). The microscopes were equipped with KEVEX analysers. For each of the samples, EDS analyses were systematically performed on numerous grains. Theoretical images were calculated with the Mac Tempas program.

The positions of the spots in electron diffraction patterns were measured from films by using a film video processor TAMRON Fotovix II X-S. This CCD image has 470000 pixel high resolution for a sixfold maximum enlargment. Each value corresponds to a minimum of 10 average measurements in the ED patterns, without any important standard deviation. All the scans were carried out following the same experimental conditions, *i.e.* increasing the temperature from 92 K to 300 K, waiting for the temperature stabilisation before each ED recording, made with a constant electron beam adjustment. For the limiting ED patterns, *i.e.* those for which the existence or non-existence of extra reflections is at the limit of detection, several exposure times were used.

The powder X-ray diffraction (XRD) data were collected with a Philips diffractometer (Cu-K$\alpha$ radiation) in the range $10° \leqslant 2\theta \leqslant 110°$ in increments of 0.02° ($2\theta$).

The resistance measurements were performed from room temperature down to 30 K, by the four probe method on sintered bars, in the earth magnetic field. All the bars have the same $2 \times 2 \times 10\ mm^3$ dimensions. The magnetisation *versus* temperature was registered during warming with a vibrating sample magnetometer, after that a magnetic field of 1.4 T or 0.01 T was applied at 4.2 K.

## Results and discussion

The magnetotransport properties of the oxides $Sm_{0.5}Ca_{0.5}Mn_{1-x}Cr_xO_3$ previously studied[16] are summarized

by the resistance measurements *versus* temperature [$R(T)$ curves] and the magnetization ones [$M(T)$ curves] displayed in Fig. 1 and 2 respectively. The examination of these curves shows that $T_{CO}$ can be deduced from the $R(T)$ curve by considering the irregularity of the curve exhibited at $T \approx 270$ K for the undoped sample (inset of Fig. 1) or by considering the bump that appears at about the same temperature on the $M(T)$ curve (inset of Fig. 2). Thus typically from the $M(T)$ curves, one can see that $T_{CO}$ decreases from 275 K for $x=0$ to 240 K for $x=0.03$ and then, no decrease of the magnetization value, which is the charge ordering (CO) signature, is shown, so that one can say that the CO has disappeared for $x \geqslant 0.05$.

Taking into consideration these results, we have performed electron microscopy structural studies from room temperature down to 92 K which is the lowest temperature that we can reach with our cooling sample holder.

### Room temperature form

At 300 K, the XRD powder patterns of the whole series ($0 \leqslant x \leqslant 0.07$) are characteristic of the classical $GdFeO_3$-type structure with an orthorhombic cell: $a \approx a_p\sqrt{2}$, $b \approx 2a_p$, $c \approx a_p\sqrt{2}$ and the space group *Pnma*. The electron diffraction investigation confirms the cell parameters and symmetry. The patterns exhibit sharp reflections, which attest to the high crystallinity of the grains. Both techniques confirm the single phase character of each sample within the $0 \leqslant x \leqslant 0.07$ domain.

The cell parameters of the undoped sample ($x=0$) were refined from XRD data (Fig. 3) to $a=5.4181(1)$ Å, $b=7.5463(3)$ Å and $c=5.3588(7)$ Å. The structure refinements lead to an $R_{Bragg}$ factor of 0.08, for the positional and thermal parameters given in Table 1. The refinements of the cell parameters of the doped materials ($0 < x \leqslant 0.07$) show no significant variation of the parameters.

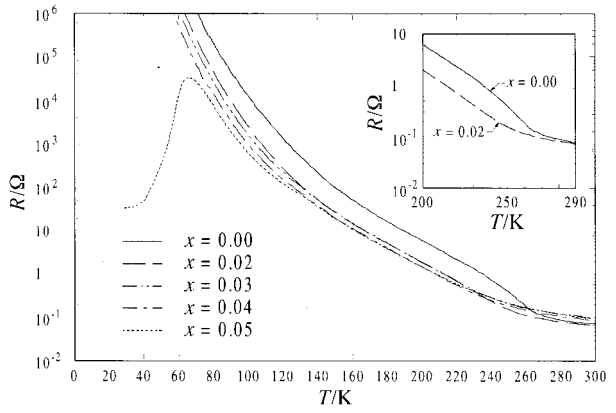


**Fig. 1** Resistance measurements *versus* temperature for the $Sm_{0.5}Ca_{0.5}Mn_{1-x}Cr_xO_3$ series with $0 \leqslant x \leqslant 0.05$. Inset: Close-up of the $R(T)$ curves of the $Sm_{0.5}Ca_{0.5}MnO_3$ and $Sm_{0.5}Ca_{0.5}Mn_{0.98}Cr_{0.02}O_3$ compounds.

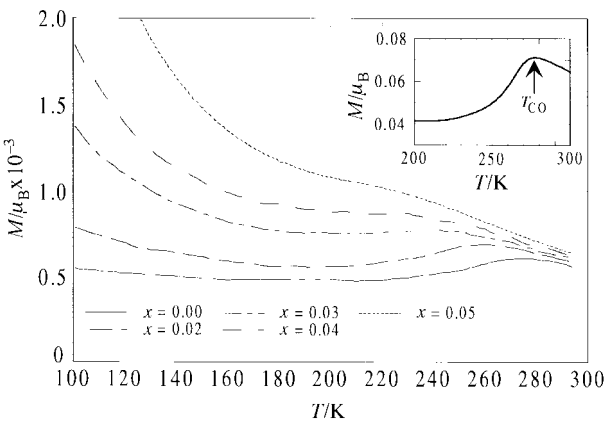


**Fig. 2** Magnetization measurements *versus* temperature registered under $10^{-2}$ T for the $Sm_{0.5}Ca_{0.5}Mn_{1-x}Cr_xO_3$ series with $0 \leqslant x \leqslant 0.05$. Inset: Close-up of the $M(T)$ curve of the $Sm_{0.5}Ca_{0.5}MnO_3$ compound ($B=1.45$ T).

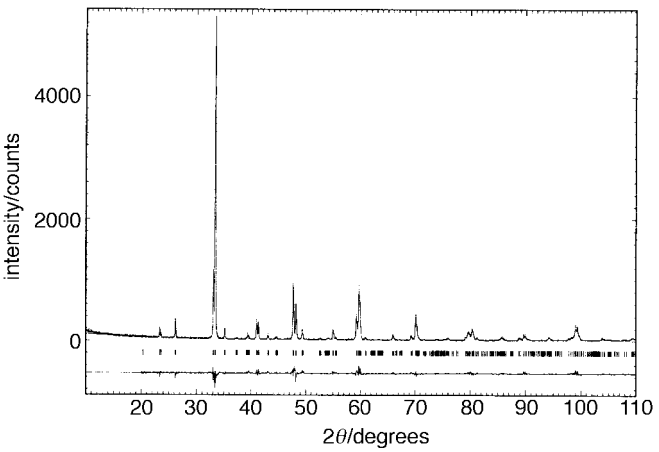


**Fig. 3** X-Ray diffraction data of the $Sm_{0.5}Ca_{0.5}MnO_3$ manganite at room temperature

The compositional homogeneity of the crystallites was checked from energy dispersive spectroscopy (EDS) analyses, carried out on about thirty grains per sample. Average Sm/Ca and (Sm + Ca)/(Mn + Cr) ratios close to 1 were systematically obtained, in the limits of accuracy of the technique. The determined average Sm and Ca content, $Sm_{0.5\pm0.02}Ca_{0.5\pm0.02}$ (where 0.02 is not the sensivity of the technique but represents the maximum experimental deviation with regard to the average value), is that of the nominal composition. The chromium doping effect was also checked by EDS: for such small $x$ values, the EDS analyses cannot provide an accurate Cr content, within a limiting deviation of 0.01 corresponding to the step of the nominal compositions, but they show that Cr has actually entered into the matrix and that $x$ regularly increases in accordance with the nominal content. This is also in agreement with the evolution of the physical properties.

The two limit compounds, *i.e.* $x=0$ and $x=0.07$, were studied by high resolution electron microscopy (HREM). Four viewing directions were selected, namely the [100], [001], [010] and [101] directions of the *Pnma*-type cell, since they allow the characterisation of the equivalent $\{110\}_p$ and $\{100\}_p$ planes of the ideal cubic perovskite cell and the directions along which most of the nanostructural features are formed.

The main features observed in the two samples can be summarised as follows. (i) In a general way, grains are very well crystallised, with very few or even no extended defects. An example of a [010] image, recorded for $x=0$, is given in Fig. 4(a), where the cation positions are imaged as bright dots. A good fit is obtained between the experimental images and the ones calculated for the positional parameter given in Table 1 [see for example Fig. 4(b) calculated for a focus value close to $-500$ Å and a crystal thickness of 23 Å, and compare with the experimental image in Fig. 4(a)]. The contrasts of the images recorded for the undoped and doped samples are very similar. (ii) The formation of 90° oriented domains, which result from the orthorhombic distortion of the *Pnma* cell, is a frequent feature. As a consequence, adjacent [100] and [001] domains on one hand, and [010] and [101] domains on the other hand, are quite systematically observed in the crystallites. This is common behaviour for the distorted perovskite-type structures. The domain boundaries are often non-planar, due to fact that the $a_o/c_o$ and $a_o\sqrt{2}/b_o$ ratios are very close to 1. The introduction of chromium into the matrix does not modify significantly this behaviour, in agreement with the cell param-

**Table 1** Structural parameters of $Sm_{0.5}Ca_{0.5}MnO_3$ at $T=300$ K (space group: *Pnma*; $a=5.4181(1)$ Å, $b=7.5463(3)$ Å, $c=5.3588(7)$ Å, $R_{Bragg}=8\%$; $\chi^2=1.71\%$)

| atom | site | $x$ | $y$ | $z$ | $B$/Å$^2$ | $n$ | bond lengths/Å |
|---|---|---|---|---|---|---|---|
| Sm/Ca | 4c | 0.0388(4) | 0.25 | −0.0081(2) | 0.15(8) | 1 | |
| Mn | 4b | 0 | 0 | 0.5 | 0.41(7) | 1 | Mn−O(1)=1.941(4) Å (2×) |
| | | | | | | | Mn−O(2)=1.938(9) Å (2×) |
| | | | | | | | Mn−O(2)=1.931(9) Å (2×) |
| O(1) | 4c | 0.4840(5) | 0.25 | 0.0834(1) | 1.0 | 1 | |
| O(2) | 8d | 0.2939(6) | 0 | −0.2939(6) | 1.0 | 2 | |

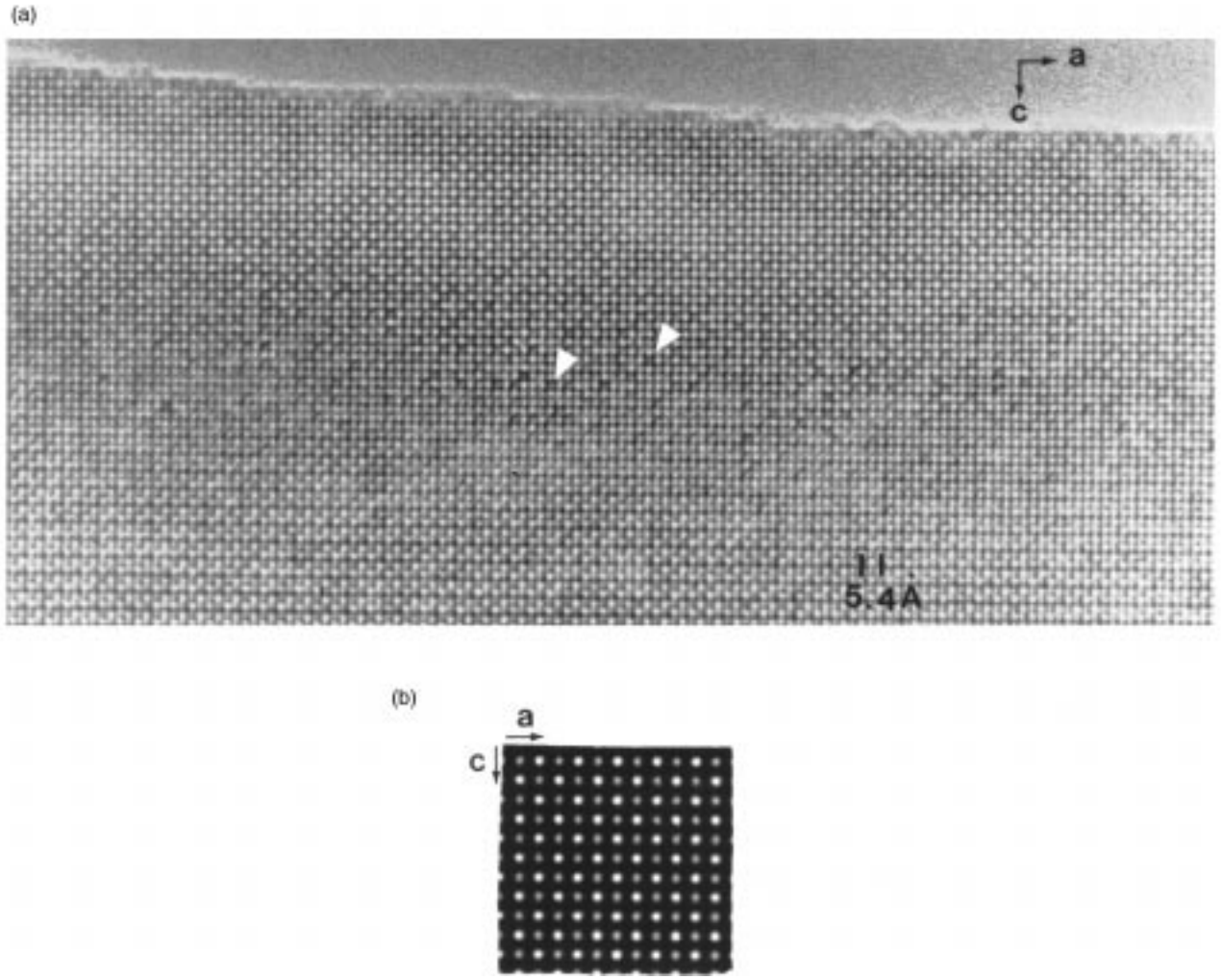


**Fig. 4** $Sm_{0.5}Ca_{0.5}MnO_3$, room temperature form: (a) [010] HREM image and (b) theoretical image for the *Pnma* structure. The focus value is close to −500 Å and the crystal thickness is 23 Å. A good fit is obtained between the experimental and calculated images. Two point-like defects are indicated, as examples, by white triangles.

eters which do not vary significantly within the $0\leqslant x\leqslant 0.07$ range. (iii) Point-like defects are observed, in the form of variations of the brightness of the dots at the level of the manganese positions and the surrounding atoms. Very often, these defects are clustered and are aligned, running over a few octahedra. Such defects were reported for the first time in the $Ln_{0.70}A_{0.30}MnO_3$ or $Ln_{0.75}A_{0.25}MnO_3$ manganites with Ln = Pr and A = Ca or Sr,[19] but they were also observed in the $Nd_{1-x}Ca_xMnO_3$ compounds with $x$ ranging from 0.3 to 0.5.[14] They were correlated to the local formation of $A^{II}Mn^{IV}O_3$ clusters.[19] The fact that they are also observed in $Sm_{0.5}Ca_{0.5}MnO_3$ confirms that it could be an intrinsic feature to these materials. However, compared to the Nd- and Pr-based samples, the density of defects seems to be smaller. Taking into consideration that these samples were prepared according to exactly the same thermal process, this suggests that the cation size could be one important parameter in the formation of such defects. Such a hypothesis needs to be confirmed by a comparative study of different $Ln_{0.5}Ca_{0.5}MnO_3$ manganites.

In the Cr doped ($x=0.07$) sample, an effect of punctual brightness variation is also clearly visible, especially along [001]. One example is given in Fig. 5(a), where the zones of light electron density are highlighted: in the thicker part of this crystal area, the $[MnO_2]_\infty$ layers appear as rows of brightest dots [compare to the theoretical image, in Fig. 5(b), calculated for a focus value close to −400 Å]. One clearly observes the variations of intensity, along [100], with one brighter dot out of two or three or four dots. These very local variations are not coherent along two adjacent rows of bright dots so that the phenomenon is not detected in the ED pattern. In that case, it is difficult to assert if the present effect is only due to the

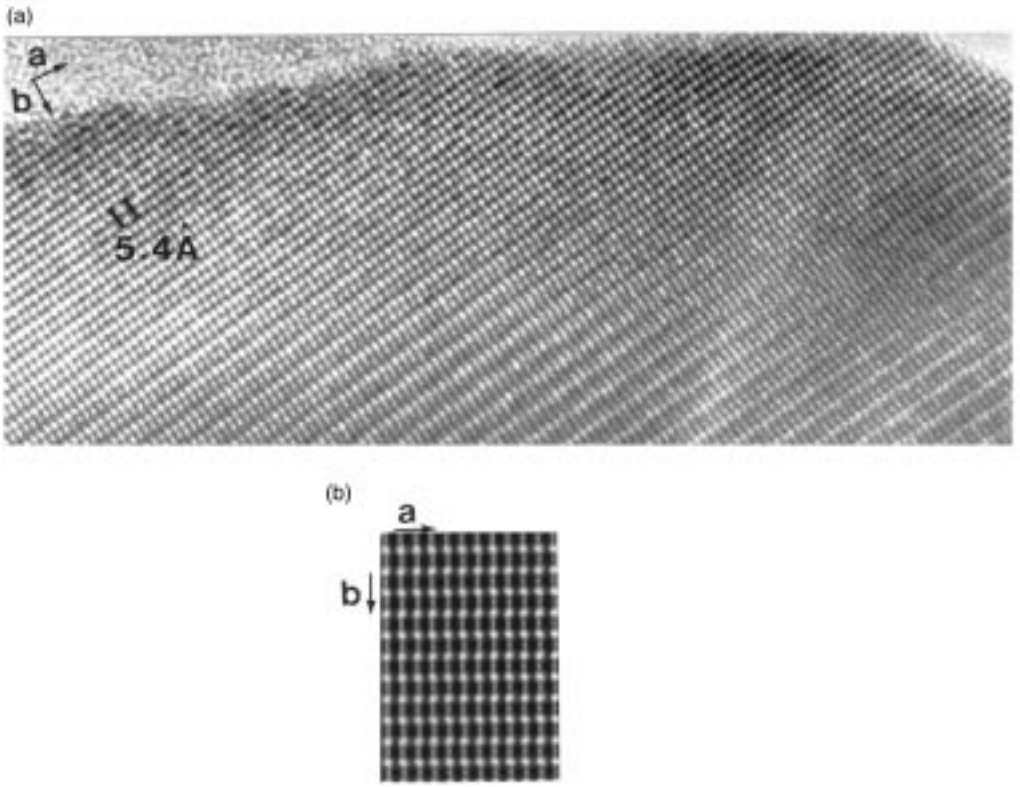


**Fig. 5** $Sm_{0.5}Ca_{0.5}Mn_{0.93}Cr_{0.07}O_3$, room temperature form: (a) [001] HREM image and (b) theoretical image. The focus value is close to −400 Å and the crystal thickness 23 Å.

formation of point-like defects similar to those observed in the undoped materials or if they are generated, or at least favoured, by the local substitution of chromium for manganese.

Thus whatever the sample, chromium doped or undoped, the classical *Pnma* structure is observed at room temperature, with only oriented domains and some local phenomena in the form of clusters.

### Low temperature form of $Sm_{0.5}Ca_{0.5}MnO_3$ ($T=92$ K)

At 92 K, all the crystallites exhibit ED patterns characterised by the presence of two systems of reflections: a first system of intense Bragg reflections which is that of the *Pnma* form, and systematically, a second system of weak extra reflections. The second system corresponds to the appearance of the reflections forbidden for the *Pnma* space group, namely $0kl$ with $k+l=2n+1$, on one hand, and of extra reflections on the other hand. For the majority of the crystallites, the extra spots are sharp and appear at positions ($\frac{1}{2}$ 0 0), implying a doubling of the $a$ parameter. Typical [010] and [001] ED patterns obtained from selected areas are given in Fig. 6(a) and (b), respectively. The cell parameters of the low temperature (LT) form are, therefore, $a\approx 2a_p\sqrt{2}$, $b\approx 2a_p$ and $c\approx a_p\sqrt{2}$. Besides these numerous crystallites, there exist some crystals with an incommensurate modulated structure at 92 K which will be studied elsewhere.[20]

The parameters of this supercell, namely the doubling of the $a$ parameter at low temperature, are similar to those reported for the other charge ordered phases $La_{0.5}Ca_{0.5}MnO_3$,[10,11] $Pr_{0.5}Ca_{0.5}MnO_3$,[1] $Tb_{0.5}Ca_{0.5}MnO_3$[13] and $Nd_{0.5}Ca_{0.5}MnO_3$.[12,14] However, the careful reconstruction of the reciprocal space of $Sm_{0.5}Ca_{0.5}MnO_3$, by tilting the crystals around different axes, selecting thin parts of the latter and the adequate zone axes to avoid double diffraction phenomena, shows that the space group of this manganite is different from those of the manganites $La_{0.5}Ca_{0.5}MnO_3$[11] and $Tb_{0.5}Ca_{0.5}MnO_3$.[13] No reflection condition for $0k0$ and $00l$ was observed and, consequently, $Sm_{0.5}Ca_{0.5}MnO_3$ does not exhibit a $2_1$ screw axis, in contrast to the manganites $Ln_{0.5}Ca_{0.5}MnO_3$ with Ln = La and Tb.[11–13] Thus, considering the orthorhombic supercell $2a_p\sqrt{2}\times 2a_p\times a_p\sqrt{2}$, the possible space groups are *Pmmm* or *P2mm*. Although no significant monoclinic distortion was detected, a monoclinic symmetry with the possible space groups *Pm* or *P2/m* cannot be ruled out. Consequently, $Sm_{0.5}Ca_{0.5}MnO_3$ exhibits the same space group as that observed for $Nd_{0.5}Ca_{0.5}MnO_3$ using convergent beam electron diffraction microscopy (CBED).[14] Note that this absence of the $2_1$ axis for $Sm_{0.5}Ca_{0.5}MnO_3$ shows that its structure is also different from those of $Nd_{1-x}Ca_xMnO_3$ oxides with $x=0.3$ and $x=0.4$, for which CBED studies[14] evidenced a similar supercell ($a=2a_p\sqrt{2}$) but with a $P2_1/m$ space group.

Owing to thermal instabilities in the microscope, high resolution images cannot be recorded at low temperature, however, the lattice images recorded at 92 K provide significant information on the way the ordering is established. An example of a [010] image is given in Fig. 6(c). One clearly observes a system of fringes: one bright fringe alternates with one less bright one (referred to as grey). The interfringe distance (*i.e.* of a double fringe [bright–grey]) is 10.8 Å, in agreement with the parameter of the 'double cell'. The system of double fringes is regularly established throughout the whole crystal, indicating long range order at low temperature.

These results show that the charge ordering observed in $Sm_{0.5}Ca_{0.5}MnO_3$ at low temperature is consistent with the 1:1 ordering of the $Mn^{3+}$ and $Mn^{4+}$ species, coupled with an orientational ordering of the $d_{z^2}$ orbitals of $Mn^{3+}$, previously proposed for various $Ln_{0.5}A_{0.5}MnO_3$ systems, and that the charge order is high at 92 K.

### Progressive charge ordered process in $Sm_{0.5}Ca_{0.5}MnO_3$: from an incommensurate to a commensurate modulated structure

The knowledge of the nature of the transition, *i.e.* the way the charge ordering proceeds as $T$ decreases or increases going

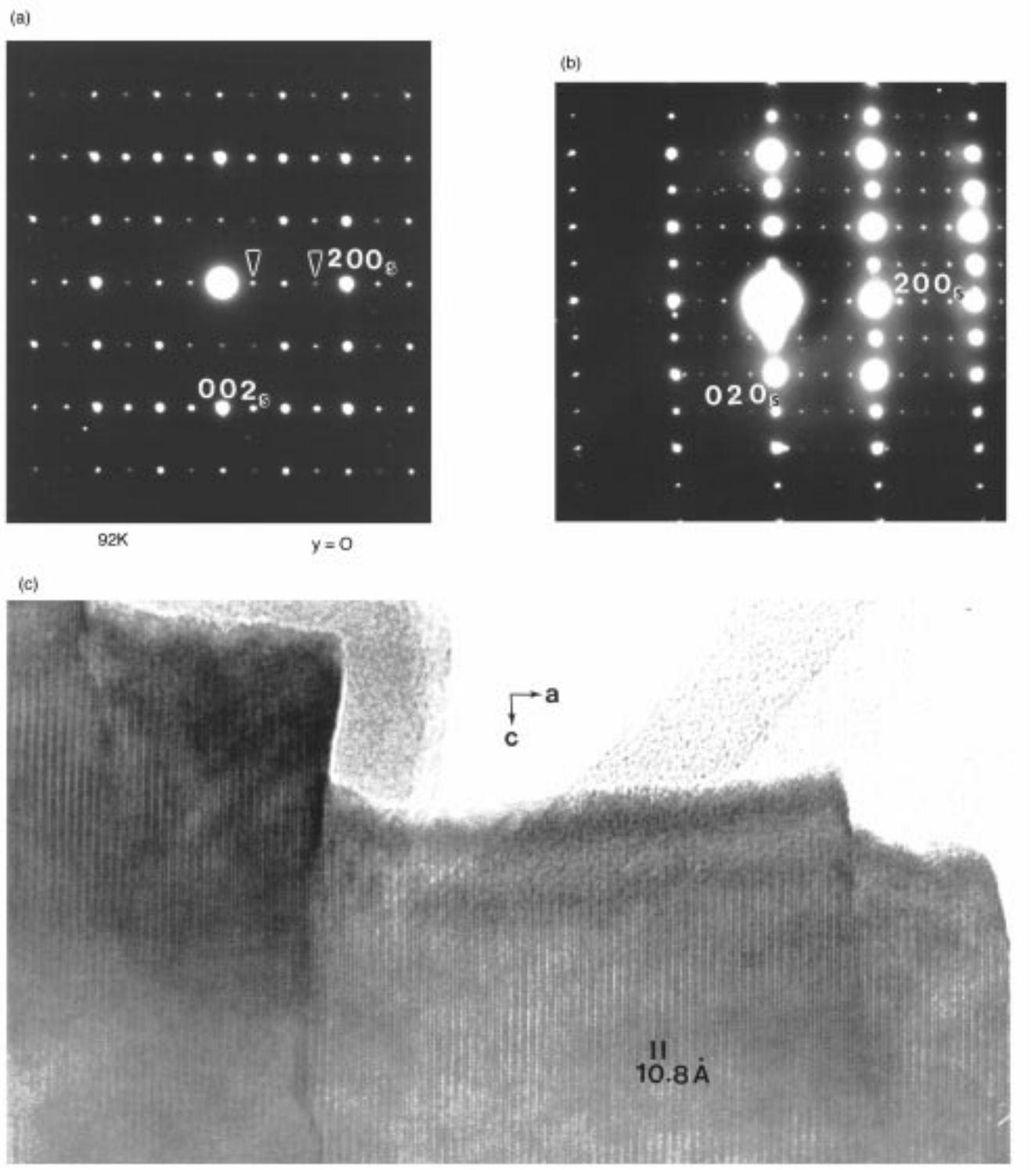


**Fig. 6** $Sm_{0.5}Ca_{0.5}MnO_3$, low temperature form ($T = 92$ K): (a) [010] and (b) [001] ED patterns are typical of the majority of the crystallites observed for $Sm_{0.5}Ca_{0.5}MnO_3$. They are indexed considering a, $a_p\sqrt{2} \times 2a_p \times a_p\sqrt{2}$ subcell (suffix s). The additional spots, indicated by triangles in the [010] pattern, are at positions (1/2 0 0) and (3/2 0 0); for the [001] pattern, the crystal was slightly tilted in order to increase the brightness of the weak extra spots. (c) [010] lattice image. The interfringe distance is 10.8 Å.

through $T_{CO}$, is an important issue for the understanding of the magnetic and transport properties of these materials. For this reason, we recorded the ED patterns of $Sm_{0.5}Ca_{0.5}MnO_3$ *versus* $T$: five selected [010] ED patterns of this phase, recorded at increasing temperature between 92 K and 300 K, are displayed in Fig. 7(a).

The extra spots, at the (1/2 0 0) positions, which are the signature of the doubling of the *a* parameter, remain unchanged up to temperatures close to 170 K. One example of an ED pattern recorded at 132 K is given in Fig. 7(a). In this figure, the extra reflections at positions ($\pm$1/2 0 $\bar{2}$), ($\overline{3/2}$ 0 $\bar{1}$) and ($\overline{1/2}$ 0 $\bar{1}$), (1/2 0 $\bar{1}$) and (3/2 0 $\bar{1}$) indicated by small white arrows, and the inter-satellite distance ($1/a_p\sqrt{2}$) between the reflections ($\overline{1/2}$ 0 $\bar{2}$) and (1/2 0 $\bar{2}$), is represented as a white horizontal bar. By increasing $T$ beyond this value, *i.e.* $T > 170$ K, one observes that the system of extra reflections is modified: this is particularly visible on the [010] ED patterns in which the satellites are rather intense. First, the extra reflections exhibit an elongated shape along [100]* of the *Pnma*-type cell, and rapid splitting of the reflections is observed [see enlarged

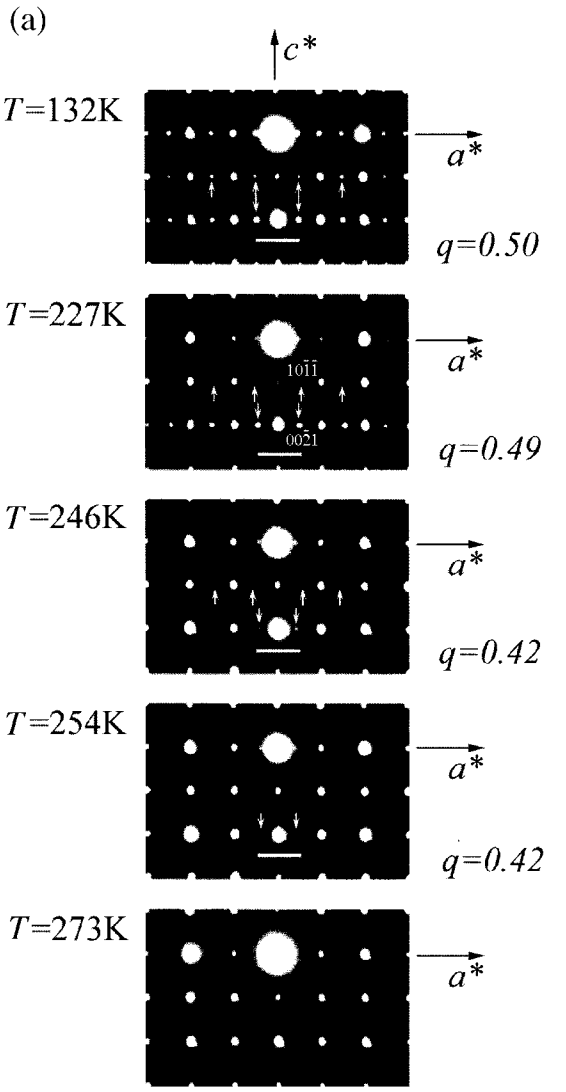


**Fig. 7** Charge ordering process in $Sm_{0.5}Ca_{0.5}MnO_3$: (a) [010] ED patterns *versus* $T$ and (b) enlargement of the ED pattern recorded at 227 K

pattern at 227 K in Fig. 7(b)], which attests to the fact that, at these temperatures, an incommensurate modulation is observed. The modulation vector is parallel to $\boldsymbol{a}^*$ and its amplitude is $q\boldsymbol{a}^*$ with $q=1/2-\delta$. Using a notation based on four indices $hklm$, the reflection at (1/2 0 0) is split into two satellites indexed (0 0 0 1) and (1 0 0 $\bar{1}$). The reconstruction of the reciprocal space shows that the conditions limiting the reflection are $hk0m$, $h=2n$, but that there is no condition for the $0k0$ and $00l$ reflections. This shows that the subcell of the incommensurate modulated structure is similar to that of the low temperature form ($T<170$ K), *i.e.* does not exhibit a screw axis $2_1$ parallel to $\boldsymbol{b}$.

The evolution of the positions of the satellites *versus* $T$ is visible in the ED patterns of Fig. 7(a) considering the shifting of the small white arrows of the (0 0 $\bar{2}$ 1) and (1 0 $\bar{1}$ $\bar{1}$) patterns which are indicated by small white arrows. The deviation with regard to the ($\pm$1/2 0 $\bar{2}$) positions, which are those of the LT form, can be directly observed thanks to the horizontal white bar. For $T>254$ K, several patterns were recorded, but the corresponding $q$ values cannot be determined since the intensity of the satellites considerably decreases and one observes the formation of nodes in diffuse streaks along $\boldsymbol{a}^*$. Then, the nodes are scarcely detectable and only diffuse streaks are observed. Finally, for $T=275$ K, extra nodes or streaks are no longer detectable and the only remaining system is the *Pnma*-type one.

The evolution of the $q$ value over the whole $T$ domain is given in Fig. 8. A first plateau is observed for $q$ values corresponding to 0.5, for $92\text{ K}\leqslant T\leqslant 170$ K. For $170\text{ K}<T<275$ K, the curve does not exhibit a regular shape but it seems that there exist two, more narrow, other plateaux, for $q=0.49$ ($\delta=0.01$) around 220 K and $q=0.42$ ($\delta=0.08$) around 250 K. The existence of these plateaux could be questionable since they may be correlated to a problem of temperature stabilisation in the electron microscope. However, for all the crystallites we have systematically observed their existence even if the corresponding $q$ values are slightly different. Such an evolution is similar to that observed for the La-based oxide $La_{0.5}Ca_{0.5}MnO_3$.[10]

Recording the ED patterns according to double temperature cycles, *i.e.* at increasing and decreasing temperatures (92 K$\rightarrow$300 K$\rightarrow$92 K$\rightarrow$300 K), shows that two successive warming scans (92 K$\rightarrow$300 K) lead to similar $q(T)$ curves. Comparison of the warming (92 K$\rightarrow$300 K) and the cooling (300 K$\rightarrow$92 K) curves shows that the transition is slightly irreversible but the plateaux are always observed.

These results show that the charge ordering process in $Sm_{0.5}Ca_{0.5}MnO_3$ is a progressive transition occurring over a large temperature range ($\Delta T=100$ K), similar to that observed in the La-based manganite.[10,11] The important point concerns the fact that the charge ordering process starts with the

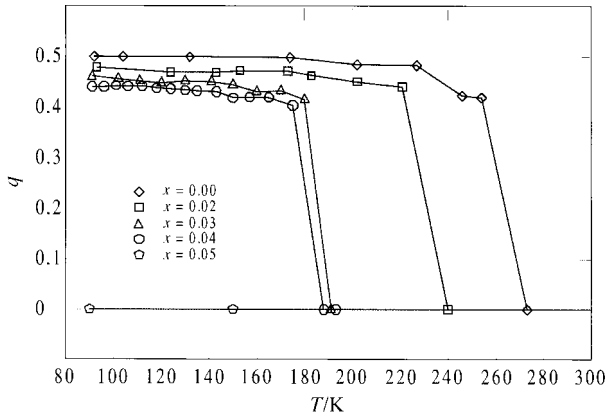


**Fig. 8** $Sm_{0.5}Ca_{0.5}Mn_{1-x}Cr_xO_3$: evolution of the $q$ value in the range $92\text{ K}\leqslant T\leqslant 300$ K

appearance of an incommensurate modulated structure at $T_{CO}=275$ K, and progressively tends toward a commensurate structure as $T$ decreases to 170 K.

The correlation of this progressive modulated charge ordering process with the $R(T)$ and $M(T)$ curves (Fig. 1 and Fig. 2) is quite remarkable. We note that the appearance of the incommensurate modulated structure at $T=275$ K for $Sm_{0.5}Ca_{0.5}MnO_3$ perfectly coincides with the slope change of the $R(T)$ curve (inset of Fig. 1). In the same way, $T=275$ K coincides with the signature of the appearance of antiferromagnetism in the $M(T)$ curve ($T_{CO}$ in inset of Fig. 2). It is also worth pointing out that the evolution of the cell parameters of this phase *versus* temperature, according to Tomioka *et al.*,[15] similarly follows a progressive variation of the parameters in the same transition zone from 275 K to 170 K. From these correlations, it clearly appears that electron microscopy is a very efficient technique, not only for characterizing $T_{CO}$, but also for indicating the width of the transition zone and the characteristic modulation vector of ordering at low temperature.

### Evolution and disappearance of the charge ordering in Cr-doped manganites

In order to check the total disappearance of the charge ordering upon chromium Mn-site doping,[16–18] a systematic exploration of the modulated structure of the doped manganites $Sm_{0.5}Ca_{0.5}Mn_{1-x}Cr_xO_3$, following the same process, has been carried out for different $x$ doping levels. These results are summarized in Fig. 8, where the $q$ value is plotted *versus* temperature for $0\leqslant x\leqslant 0.05$. These results allow the following comments to be made. (i) Starting from room temperature, the appearance of the first extra satellites as $T$ decreases leads to $T_{CO}$ values which are in perfect agreement with the values previously deduced from the $R(T)$ and $M(T)$ measurements. Thus this study confirms that $T_{CO}$ decreases as $x$ increases and that charge ordering disappears rapidly as the chromium content reaches the $x$ value of 0.05. No satellites are observed for the latter composition in agreement with the fact that the $R(T)$ curve (Fig. 1) indicates a metal to insulator transition, and that the $M(T)$ curve (Fig. 2) shows ferromagnetic behavior at low temperature and the complete absence of a bump which would be characteristic of charge ordering. (ii) The different $q(T)$ curves are similar to that of the undoped phase: the existence of a plateau at low temperature which corresponds to the $q$ value at 92 K, then a decrease of $q$ as $T$ increases to $T_{CO}$, and finally the restoration of the *Pnma*-type structure above $T_{CO}$. Note however that the temperature at which the plateau starts varies with $x$, like $T_{CO}$, so that the transition zone of the charge ordering process is quite constant in reduced temperature ($T/T_{CO}$) scale as the doping ($x$) increases. (iii) The reconstruction of the reciprocal space was carried out for the different $x$ values. They show that the conditions which are limiting the reflection are similar to those observed for the undoped phase. The $q$ value of the low temperature form (at $T=92$ K) decreases regularly as the chromium doping ($x$) increases. For $x=0.02$, 0.03 and 0.04 the $q$ values are 0.47, 0.45 and 0.44 respectively. This suggests that the undoped phase corresponding to $x=0$ is also a modulated structure, but is commensurate *i.e.* with $q=0.5$.

## Conclusion

This study of the oxides $Sm_{0.5}Ca_{0.5}Mn_{1-x}Cr_xO_3$ shows that the ordering process that takes place in these compounds is progressive and corresponds to a broad transition from an incommensurate to a commensurate modulated structure, the incommensurability $q$ vector varying from 0.40 to 0.50 at low temperature for the different chromium contents. The particular study of the $0<x\leqslant 0.05$ chromium doped compounds proves for the first time that the chromium doping increases the incommensurability of the structure at low temperature and finally leads to the total disappearance of the charge ordering phenomena for $x=0.05$. The ordering process of the undoped phase, *i.e.* the evolution of the $q$ value of $Sm_{0.5}Ca_{0.5}MnO_3$ *versus* $T$, is similar to that observed for the $La_{0.5}Ca_{0.5}MnO_3$ compound.[10,11] However, the reconstruction of the reciprocal space, carried out for the different $x$ values and at different temperatures, confirms the absence of a screw $2_1$ axis. A systematic study of these systems for different compositions, *versus* temperature and chemical parameters, coupling neutron diffraction and electron microscopy will be necessary to understand the relationship between the structure and the magnetotransport properties of these oxides.

### References


1 Z. Jirak, S. Krupicka, Z. Simsa, M. Dlouha and S. Vratislav, *J. Magn. Magn. Mater*., 1985, **53**, 153.
2 Y. Tomioka, A. Asamitsu, Y. Moritomo, H. Kuwahara and Y. Tokura, *Phys. Rev. Lett*., 1995, **74**, 5108.
3 Y. Tokura, H. Kuwahara, Y. Moritomo, Y. Tomioka and A. Asamitsu, *Phys. Rev. Lett*., 1996, **76**, 3184.
4 V. Caignaert, F. Millange, M. Hervieu, E. Suard and B. Raveau, *Solid State Commun*., 1996, **99**, 173.
5 J. Wolfman, Ch. Simon, M. Hervieu, A. Maignan and B. Raveau, *J. Solid State Chem*., 1996, **123**, 413.
6 J. Wolfman, A. Maignan, Ch. Simon and B. Raveau, *J. Magn. Magn. Mater*., 1996, **159**, L299.
7 N. Kumar and C. N. R. Rao, *J. Solid State Chem*., 1997, **129**, 363.
8 F. Damay, A. Maignan, C. Martin and B. Raveau, *J. Appl. Phys*., 1997, **81**, 1372.
9 F. Damay, C. Martin, A. Maignan and B. Raveau, *J. Appl. Phys*., 1997, **82**, 618.
10 C. H. Chen and S. W. Cheong, *Phys. Rev. Lett*., 1996, **76**, 4042.
11 P. G. Radaelli, D. E. Cox, M. Marezio and S. W. Cheong, *Phys. Rev. B*, 1997, **55**, 3015.
12 T. Vogt, A. K. Cheetham, R. Mahendiran, A. K. Raychaudhuri, R. Mahesh and C. N. R. Rao, *Phys. Rev. B*, 1996, **54**, 15 303.
13 J. Blasco, J. Garcia, J. M. De Teresa, M. R. Ibarra, J. Perez, P. A. Algarabel, C. Marquina and C. Ritter, *J. Phys. Condens. Matter*, 1997, **9**, 10 321.
14 O. Richard, W. Schuddinck, G. Van Tendeloo, F. Millange, M. Hervieu, V. Caignaert and B. Raveau, *Phys. Rev. B*, submitted.
15 Y. Tomioka, A. Asamitsu, H. Kuwahara, Y. Moritomo, M. Kasai, R. Kumai and Y. Tokura, *Physica B*, 1997, **237**, 1.
16 A. Barnabé, A. Maignan, M. Hervieu, F. Damay, C. Martin and B. Raveau, *Appl. Phys. Lett*., 1997, **71**, 3907.
17 A. Maignan, F. Damay, C. Martin and B. Raveau, *Mater. Res. Bull*., 1997, **32**, 965.
18 B. Raveau, A. Maignan and C. Martin, *J. Solid State Chem*., 1997, **130**, 162.
19 M. Hervieu, G. Van Tendeloo, V. Caignaert, A. Maignan and B. Raveau, *Phys. Rev. B*, 1996, **53**, 14 274.
20 A. Barnabé, M. Hervieu, C. Martin, A. Maignan and B. Raveau, *J. Appl. Phys*., submitted.


*Paper* 8/00994E; *Received* 4*th February*, 1998